Chinese Chemical Letters 34 (2023) 108093

Contents lists available at ScienceDirect

Chinese Chemical Letters

journal homepage: www.elsevier.com/locate/cclet

Ratiometric fluorescence and visual sensing of ATP based on gold nanocluster-encapsulated metal-organic framework with a smartphone

Xiaomeng Zhou[a], Xinjie Wang[b], Li Shang[a,c,*]

[a] State Key Laboratory of Solidification Processing, School of Materials Science and Engineering, Northwestern Polytechnical University and Shaanxi Joint Laboratory of Graphene (NPU), Xi'an 710072, China
[b] Queen Mary University of London Engineering School, Northwestern Polytechnical University, Xi'an 710072, China
[c] NPU-QMUL Joint Research Institute of Advanced Materials and Structures (JRI-AMAS), Northwestern Polytechnical University, Xi'an 710072, China

ARTICLE INFO

Article history:
Received 14 September 2022
Revised 16 December 2022
Accepted 21 December 2022
Available online 24 December 2022

Keywords:
Gold nanoclusters
Fluorescence sensors
Metal-organic frameworks
ATP

ABSTRACT

Adenosine triphosphate (ATP) plays an important role in various biological processes and the ATP level is closely associated with many diseases. Herein, we designed a novel dual-emissive fluorescence nanoplatform for ATP sensing based on red emissive europium metal-organic framework (Eu-MOF) and blue emissive gold nanoclusters (AuNCs). The presence of ATP causes the decomposition of Eu-MOF owing to strong affinity of Eu^{3+} with ATP. As a result, the red emission of Eu-MOF decreases while the blue emission of AuNCs remains unchanged. The distinct red/blue emission intensity change enables the establishment of a ratiometric fluorescent and visual sensor of ATP. Moreover, a fluorescent paper-based sensor was fabricated with the ratiometric ATP probes, which enabled easy-to-use and visual detection of ATP in serum samples with a smartphone.

Adenosine 5′-triphosphate (ATP) is not only the primary energy source for cellular processes, but also plays an important role in various biological processes including intracellular energy transfer, signal transduction, DNA replication and membrane transport [1–4]. The abnormal level of ATP is typically closely associated with many diseases such as hypoglycemia [5], Alzheimer's disease and malignant tumors [6,7]. Therefore, selective detection and accurate quantification of ATP in biological samples is extremely important. Many approaches have been developed for ATP detection, such as surface plasmon resonance [8,9] chemiluminescence [10], surface enhanced Raman scattering [11–13], colorimetric [14,15], and electrochemical approaches [16,17]. However, these methods often need sophisticated operation, require high-cost equipment and time-consuming analysis. Fluorescence assays have received considerable attention in the field of ATP sensing due to their simplicity, rapid response and high sensitivity [18–24]. While many fluorescent ATP sensors have been developed in recent years, it still remains challenging to achieve visual and on-site detection of ATP which largely restricts their practical application.

Paper-based analytical devices have been widely used for molecular analysis, health and environmental monitoring recently due to their low cost, portability and disposability [25–27]. For example, Luo *et al.* [28] synthesized a dual-state emissive chalcone probe with the feature of aggregation-induced emission and loaded the probe into test papers. The obtained fluorescent test papers were successfully employed for human serum albumin test using the whole blood samples. Wang *et al.* developed a paper-based analytical device with dual-emission carbon dots for the on-site and semiquantitative detection of lead ions in water samples [29]. Importantly, paper-based sensors enable low-cost, sensitive and instant naked eye detection of analytes. Nevertheless, there are few reports about fluorescent paper-based platforms for ATP sensing, which is mainly due to the lack of robust probes.

Noble metal nanoclusters have recently emerged as promising fluorescent nanoprobes for biosensing and bioimaging duo to their ultrasmall core size (<2 nm), strong photoluminescence, facile availability, and good biocompatibility [30,31]. Metal-organic frameworks (MOFs) have also been explored as excellent sensing materials because of their porous nature, adjustable functionality, and unique optical properties [32,33]. The combination of AuNCs and luminescent MOFs can not only provide multiple emission centers but also endow the MOF/AuNCs assemblies with enhanced selectivity, sensitivity, and stability for fluorescent sensing [26,34]. Herein, we propose a novel paper-based visual and fluorescent

* Corresponding author at: State Key Laboratory of Solidification Processing, School of Materials Science and Engineering, Northwestern Polytechnical University and Shaanxi Joint Laboratory of Graphene (NPU), Xi'an 710072, China.
E-mail address: li.shang@nwpu.edu.cn (L. Shang).

https://doi.org/10.1016/j.cclet.2022.108093
1001-8417/

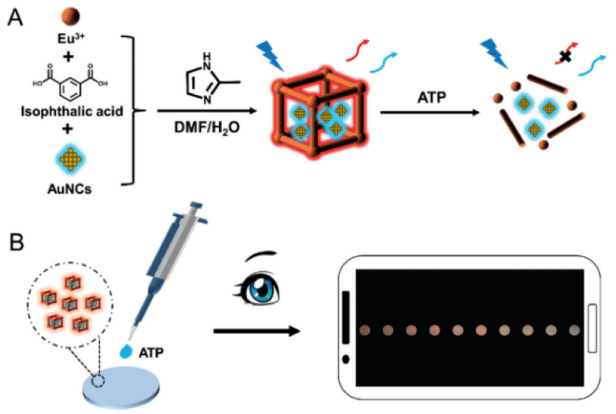

Scheme 1. Schematic illustration of the fabrication of BSA-AuNCs@Eu-MOF-based ATP nanosensors (A) and further development of paper-based sensors for visual ATP detection (B).

ATP sensing platform based on ratiometric luminescent nanoprobes by integrating fluorescent gold nanoclusters (AuNCs) with MOFs. As described in Scheme 1, a ratiometric fluorescent ATP sensor was fabricated by encapsulating blue emissive gold nanoclusters (AuNCs, as the reference signal) into red emissive lanthanide metal-organic frameworks (Eu-MOF, as the response signal), which possess dual emission feature and good stability. Introduction of ATP could trigger the decomposition of AuNCs@Eu-MOF nanocomposites owing to competitive binding of Eu^{3+} with ATP. Consequently, the red fluorescence of Eu-MOF decreased, while the blue fluorescence of AuNCs is inert to the presence of ATP. Therefore, quantitative fluorescent analysis of ATP can be achieved. Moreover, AuNCs@Eu-MOF probes were loaded into fluorescent test papers, which can be used to detect ATP based on the fluorescence change of the test paper with a smartphone under a UV lamp. Thereby, this study provides a new strategy to enable fluorescent and visual detection of ATP for on-site clinical analysis.

AuNCs@Eu-MOF composites were prepared through self-assembly using isophthalic acid and Eu^{3+} as the precursors of MOF in the presence of bovine serum albumin-protected AuNCs (BSA-AuNCs). BSA-AuNCs were first synthesized according to reported strategy [35]. 2-Methylimidazole was then added to trigger the nucleation to construct AuNCs@Eu-MOF at room temperature [36]. As shown in Fig. 1A, AuNCs@Eu-MOF exhibits regular fusiform shape with an approximate length of 5 μm. Compared with pure Eu-MOF with a smooth surface (Fig. S1 in Supporting information), the surface of AuNCs@Eu-MOF was coarse, which is likely due to the attachment of BSA-AuNCs on the MOF surface. Fourier-transform infrared spectroscopy (FTIR, Fig. 1B) further showed that, distinct peaks of BSA-AuNCs at 1656 and 1540 cm^{-1} corresponding to the characteristic stretching and bending vibrations of amide I, amide II in BSA, respectively, were maintained in the AuNCs@Eu-MOF composites [35]. Moreover, peaks of BSA-AuNCs at 1240 and 1046 cm^{-1} disappeared after combination with Eu-MOF, which is likely due to the shielding effect of Eu-MOF nanocrystals [37]. XRD analysis further confirmed the crystal structure of AuNCs@Eu-MOF. As shown in Fig. 1C, the negligible effect of AuNCs on structure of Eu-MOF was verified by the similarity of diffraction peaks of AuNCs@Eu-MOF as the pure Eu-MOF. To further confirm the successful assembly of AuNCs and Eu-MOF, thermogravimetric analysis (TGA) was carried out. TGA results showed that AuNCs@Eu-MOF possesses a much higher decomposition temperature than Eu-MOF. The weight loss at 1000 °C refers to the Au content in AuNCs@Eu-MOF (Fig. 1D), which is due to the existence of Au element that strengthens the thermal stability of whole framework. All these results confirm that AuNCs were successfully incorporated into Eu-MOF.

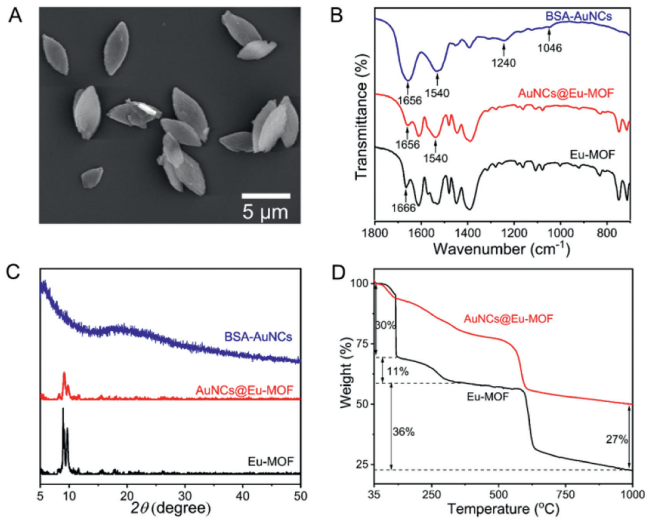

Fig. 1. (A) SEM image of AuNCs@Eu-MOF; FTIR spectra (B) and XRD patterns (C) of BSA-AuNCs, Eu-MOF and AuNCs@Eu-MOF; (D) TGA curves of Eu-MOF and AuNCs@Eu-MOF.

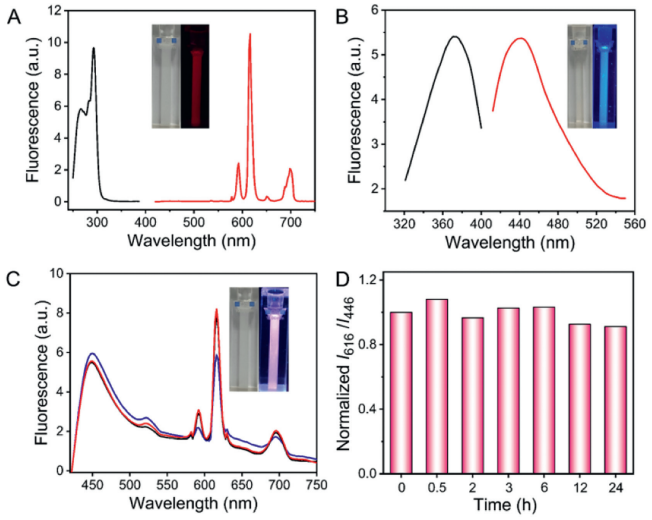

Fig. 2. Excitation (black) and emission (red) spectra of Eu-MOF (A) and BSA-AuNCs (B) in aqueous solution; (C) fluorescence emission spectra of AuNCs@Eu-MOF with different molar ratios of AuNCs to Eu^{3+}: 80:1 (blue), 40:1 (red), and 20:1 (black); (D) fluorescence stability of AuNCs@Eu-MOF (40:1) *versus* the time in the aqueous solution. Excitation wavelength: 365 nm.

We then studied the optical properties of as-prepared AuNCs@Eu-MOF. Before the assembly, BSA-AuNCs exhibit strong blue fluorescence with the emission peak at 446 nm, and Eu-MOF exhibits characteristic red emission of Eu^{3+} with the emission peak at 616 nm owing to the antenna effect (Figs. 2A and B). As shown in Fig. 2C, the formed AuNCs@Eu-MOF showed emissive features of both BSA-AuNCs and Eu^{3+}. Particularly, the dual emission intensity was strongly dependent on the ratio of AuNCs to Eu^{3+}, and the intensity ratio of Eu-MOF to AuNCs (I_{616}/I_{446}) reached maximum when the ratio of AuNCs to Eu^{3+} is 40:1. With increasing the concentration of AuNCs in the synthetic procedure, a slight decrease in the emission band of Eu-MOF was observed, which might be due to the coordination of carboxylate groups in BSA-AuNCs with Eu^{3+} centers. This might induce less energy transfer efficiency from the initial ligand isophthalic acid (ISP) to Eu^{3+} according to the antenna effect, thus decreasing the Eu^{3+} characteristic emission [38].

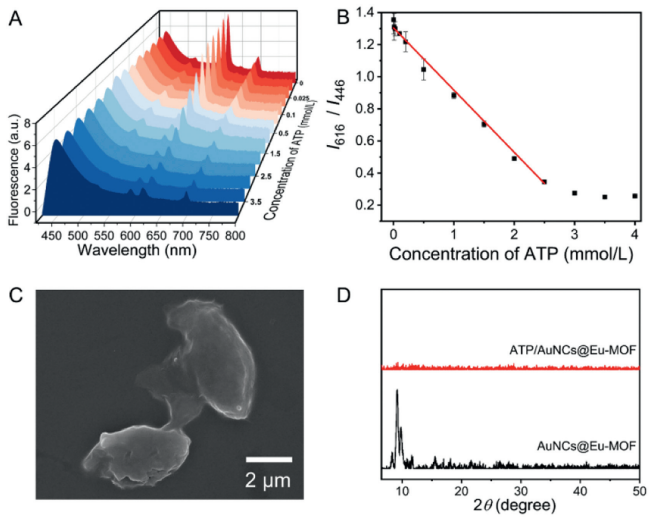

Fig. 3. (A) Fluorescence emission spectra of AuNCs@Eu-MOF with the addition of increasing concentrations of ATP. Excitation wavelength: 365 nm; (B) changes of the I_{616}/I_{446} value *versus* the ATP concentration. Red line denotes the linear fit in the range of 0.01 mmol/L to 2.5 mmol/L; (C) SEM images of AuNCs@Eu-MOF in the presence of ATP; (D) PXRD patterns of AuNCs@Eu-MOF in the absence (black) and presence (red) of ATP.

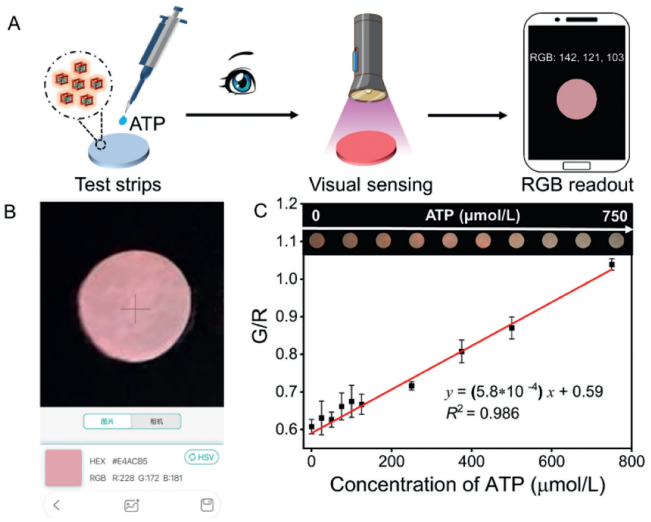

Fig. 4. (A) Schematic diagram for the detection of ATP using a smartphone; (B) the photo of a smartphone installed with a color recognition App; (C) color change of test stripes (green channel/red channel) *versus* the concentration of ATP (the insets show photos that were taken with a smartphone under a 310 nm UV lamp).

The effect of AuNCs on Eu-MOF emission further confirms the successful assembly of AuNCs and Eu-MOF. We also investigated the fluorescence stability of AuNCs@Eu-MOF in aqueous solution. The fluorescence intensity of AuNCs@Eu-MOF in Tris–HCl (pH 7.4) kept almost unchanged within 24 h, indicating a good stability (Fig. 2D).

Next we evaluated the fluorescence response of AuNCs@Eu-MOF towards ATP. The reaction time was optimized to acquire the best sensing performance as shown in Fig. S2 (Supporting information). With extending the reaction time, the I_{446}/I_{616} value increased rapidly and reached maximum in 10 min. As expected, red Eu^{3+} emission gradually decreased while the blue BSA-AuNCs emission remain constant as the concentration of ATP increased (Fig. 3A). A good linear relationship ($R^2 = 0.998$) between the I_{616}/I_{446} value and ATP concentration in a wide range of 0.01 mmol/L to 2.5 mmol/L was obtained, and as low as 10 μmol/L could be detected (Fig. 3B), which is far below the physiological concentration of ATP (0.4–3.7 mmol/L). The sensitivity of our approach is comparable or even better than many nanomaterial-based fluorescent sensors (Table S2 in Supporting information) [39–41]. This suggests that our ratiometric fluorescence sensor could be utilized for ATP detection in real samples [42,43].

It has been previously reported that trivalent lanthanide ions (Ln^{3+}) possess high affinity for oxygen-donor atoms, especially phosphates [44,45]. Therefore, addition of ATP could displace ISP from Eu-MOF, leading to the collapse of the Eu-MOF framework. As a result, energy transfer between ISP and Eu^{3+} was blocked and the red Eu^{3+} emission decreased. Meanwhile, the fluorescence of BSA-AuNCs was not affected upon the addition of ATP (Fig. S3 in Supporting information). As a result, the red emission intensity changed significantly after the addition of ATP, which can be used for developing a ratiometric fluorescent ATP sensor with the blue emission of AuNCs as the self-reference. As seen in Fig. 3C, the ATP treatment resulted in partial melting of AuNCs@Eu-MOF due to the degradation of MOF structures. Moreover, the disappearance of XRD peaks of Eu-MOF in the presence of ATP further confirmed the proposed sensing mechanism (Fig. 3D).

The selectivity of AuNCs@Eu-MOF for ATP towards other potential interferences was investigated. As shown in Fig. S4 (Supporting information), for GTP, UTP and CTP which also have three phosphate groups, a slight increase in the I_{446}/I_{616} value could also be observed. Since the ATP level in biological fluids is of a greater amount than other triphosphate-containing species, their possible interference on the detection of ATP is negligible [5,46]. Thus this ratiometric fluorescence assay can provide a good selectivity for further ATP sensing in real samples.

To further facilitate on-site visualization of ATP in practical applications, the above ratiometric fluorescent probes, AuNCs@Eu-MOF, were loaded into paper substrate. As shown in Fig. 4A, when aqueous solution of ATP drops onto the test strips, the color of the paper-based ATP sensor gradually changed from pink to light blue under a UV lamp with an increase of ATP concentration from 0 to 750 μmol/L. To quantitate the ATP concentration using our fluorescent paper sensor, the color information (RGB values) of the paper sensor was read by a smartphone application (Fig. 4B). As shown in Fig. 4C, the ratio of green channel to red channel has a good linear relationship ($R^2 = 0.986$) with the ATP concentration within the range of 25–750 μmol/L. These results suggest that our fluorescent paper sensor can realize portable quantitative detection of ATP simply with a smartphone. Furthermore, human serum (10%) spiked with ATP of different concentrations was used as real samples to validate the practical potential of this fluorescent paper sensor. The recovery rates in human serum calculated by RGB value were found to be 93.5%–120.5% (Table S1 in Supporting information). These results demonstrate that our smartphone-based fluorescent paper sensor has great potential for the visual ATP sensing in biological complex samples.

In summary, we have developed a novel ratiometric fluorescence assay for the detection of ATP based on ATP-triggered decomposition of AuNCs@Eu-MOF. The presence of ATP could displace ISP from Eu-MOF, leading to the collapse of the Eu-MOF framework. As a result, the red Eu^{3+} emission decreased gradually while the blue BSA-AuNCs emission remains constant. Consequently, a ratiometric fluorescent sensor for ATP can be established, which showed competitive sensitivity and selectivity towards ATP sensing. Moreover, a fluorescent paper-based sensor was fabricated with these novel probes to render a simple, visual assay of ATP in human serum, and satisfactory results were obtained. We envision that the present visual sensing strategy could provide useful guidelines for further developing novel optical biosensors.

Declaration of competing interest

The authors declare that they have no known competing financial interests or personal relationships that could have appeared to influence the work reported in this paper.

Acknowledgments

This work is supported by the National Natural Science Foundation of China (No. 22274131) and the Research Fund of the State Key Laboratory of Solidification Processing (NPU), China (No. 2020-QZ-01).

Supplementary materials

Supplementary material associated with this article can be found, in the online version, at doi:10.1016/j.cclet.2022.108093.

References

[1] Z. Gao, Z. Qiu, M. Lu, J. Shu, D. Tang, Biosens. Bioelectron. 89 (2017) 1006–1012.
[2] X. Shen, G. Mizuguchi, A. Hamiche, C. Wu, Nature 406 (2000) 541–544.
[3] P.B. Dennis, A. Jaeschke, M. Saitoh, et al., Science 294 (2001) 1102–1105.
[4] M. Mei, L. Mu, Y. Wang, et al., Anal. Chem. 94 (2022) 11813–11820.
[5] P.K. Yeung, S.S. Kolathuru, S. Mohammadizadeh, F. Akhoundi, B. Linderfield, Metabolites 8 (2018) 30–43.
[6] S.L. Cai, Y.B. Zheng, S.H. Cao, X.H. Cai, Y.Q. Li, Chem. Commun. 52 (2016) 12450–12453.
[7] J.K. Ahn, H.Y. Kim, K.S. Park, H.G. Park, Anal. Chem. 90 (2018) 11340–11343.
[8] J.H. Park, J.Y. Byun, W.B. Shim, S.U. Kim, M.G. Kim, Biosens. Bioelectron. 73 (2015) 26–31.
[9] L. Xie, X. Yan, Y. Du, Biosens. Bioelectron. 53 (2014) 58–64.
[10] Y.P. Dong, Y. Zhou, J. Wang, J.J. Zhu, Anal. Chem. 88 (2016) 5469–5475.
[11] H. Shi, N. Chen, Y. Su, H. Wang, Y. He, Anal. Chem. 89 (2017) 10279–10285.
[12] X. Zhang, Y. Ge, M. Liu, et al., Anal. Chem. 94 (2022) 7823–7832.
[13] C. Wu, S. Wang, X. Luo, R. Yuan, X. Yang, Chem. Commun. 56 (2020) 1413–1416.
[14] D. Cheng, Y. Li, J. Wang, et al., Chem. Commun. 51 (2015) 8544–8546.
[15] S. Li, X. Zhao, X. Yu, et al., Anal. Chem. 91 (2019) 14737–14742.
[16] G. Wang, Q. Xu, L. Liu, et al., ACS Appl. Mater. Interfaces 9 (2017) 31153–31160.
[17] J. Zheng, X. Li, K. Wang, J. Song, H. Qi, Anal. Chem. 92 (2020) 10940–10945.
[18] C. Qin, Y. Li, Q. Li, C. Yan, L. Cao, Chin. Chem. Lett. 32 (2021) 3531–3534.
[19] Z. Wu, M. Liu, Z. Liu, Y. Tian, J. Am. Chem. Soc. 142 (2020) 7532–7541.
[20] X. Zhou, L. Shang, Curr. Anal. Chem. 18 (2022) 677–688.
[21] Y. Zhong, T. Yi, J. Mater. Chem. B 7 (2019) 2549–2556.
[22] K. Fan, S.S. Bao, W.X. Nie, C.H. Liao, L.M. Zheng, Inorg. Chem. 57 (2018) 1079–1089.
[23] Y. Wu, J. Wen, H. Li, S. Sun, Y. Xu, Chin. Chem. Lett. 28 (2017) 1916–1924.
[24] X. Shi, H. Xu, Y. Wu, et al., J. Anal. Test. 5 (2021) 165–173.
[25] X. Lyu, V. Hamedpour, Y. Sasaki, Z. Zhang, T. Minami, Anal. Chem. 93 (2021) 1179–1184.
[26] Q. Gao, S. Xu, C. Guo, Y. Chen, L. Wang, ACS Appl. Mater. Interfaces 10 (2018) 16059–16065.
[27] W. Li, X. Zhang, S. Chen, Y. Ji, R. Li, Chin. Chem. Lett. 33 (2022) 4405–4410.
[28] Z. Luo, T. Lv, K. Zhu, et al., Angew. Chem. Int. Ed. 59 (2020) 3131–3136.
[29] H. Wang, L. Yang, S. Chu, et al., Anal. Chem. 91 (2019) 9292–9299.
[30] Z.J. Wang, Q. Li, L.L. Tan, C.G. Liu, L. Shang, J. Anal. Test. 6 (2022) 163–177.
[31] J. Xu, J. Li, W. Zhong, et al., Chin. Chem. Lett. 32 (2021) 2390–2394.
[32] X. Zhou, J. Li, L.L. Tan, Q. Li, L. Shang, J. Mater. Chem. B 8 (2020) 3661–3666.
[33] S. Wu, H. Min, W. Shi, P. Cheng, Adv. Mater. 32 (2020) e1805871.
[34] X. Yin, B. Yang, B. Chen, M. He, B. Hu, Anal. Chem. 91 (2019) 10596–10603.
[35] X.Le Guével, B. Hötzer, G. Jung, et al., J. Phys. Chem. C 115 (2011) 10955–10963.
[36] C. Guo, Y. Zhang, Y. Guo, et al., Chem. Commun. 54 (2018) 252–255.
[37] Z. Wu, H. Yang, S. Pan, H. Liu, X. Hu, ACS Sens. 5 (2020) 2211–2220.
[38] Z.R. Yang, M.M. Wang, X.S. Wang, X.B. Yin, Anal. Chem. 89 (2017) 1930–1936.
[39] X. Zheng, R. Peng, X. Jiang, et al., Anal. Chem. 89 (2017) 10941–10947.
[40] K. Wang, M. Qian, H. Qi, Q. Gao, C. Zhang, Nanoscale 12 (2020) 15663–15669.
[41] W. Qiang, H. Hu, L. Sun, H. Li, D. Xu, Anal. Chem. 87 (2015) 12190–12196.
[42] M. Liu, X. Ren, X. Liu, et al., Chin. Chem. Lett. 31 (2020) 3117–3120.
[43] R. Mo, T. Jiang, R. DiSanto, W. Tai, Z. Gu, Nat. Commun. 5 (2014) 3364–3373.
[44] H. He, C. Li, Y. Tian, P. Wu, X. Hou, Anal. Chem. 88 (2016) 5892–5897.
[45] S.M. Harris, J.T. Nguyen, S.L. Pailloux, et al., Environ. Sci. Technol. 51 (2017) 4549–4558.
[46] V. Vultaggio-Poma, A.C. Sarti, F. Di Virgilio, Cells 9 (2020) 2496–2517.